© 2015. Published by The Company of Biologists Ltd | Journal of Cell Science (2015) 128, 3435-3443 doi:10.1242/jcs.172031

RESEARCH ARTICLE

Vinculin phosphorylation at residues Y100 and Y1065 is required for cellular force transmission

Vera Auernheimer[1], Lena A. Lautscham[1], Maria Leidenberger[2], Oliver Friedrich[2], Barbara Kappes[2], Ben Fabry[1] and Wolfgang H. Goldmann[1,*]

ABSTRACT

The focal adhesion protein vinculin connects the actin cytoskeleton, through talin and integrins, with the extracellular matrix. Vinculin consists of a globular head and tail domain, which undergo conformational changes from a closed auto-inhibited conformation in the cytoplasm to an open conformation in focal adhesions. Src-mediated phosphorylation has been suggested to regulate this conformational switch. To explore the role of phosphorylation in vinculin activation, we used knock-out mouse embryonic fibroblasts re-expressing different vinculin mutants in traction microscopy, magnetic tweezer microrheology, FRAP and actin-binding assays. Compared to cells expressing wild-type or constitutively active vinculin, we found reduced tractions, cytoskeletal stiffness, adhesion strength, and increased vinculin dynamics in cells expressing constitutively inactive vinculin or vinculin where Src-mediated phosphorylation was blocked by replacing tyrosine at position 100 and/or 1065 with a non-phosphorylatable phenylalanine residue. Replacing tyrosine residues with phospho-mimicking glutamic acid residues restored cellular tractions, stiffness and adhesion strength, as well as vinculin dynamics, and facilitated vinculin–actin binding. These data demonstrate that Src-mediated phosphorylation is necessary for vinculin activation, and that phosphorylation controls cytoskeletal mechanics by regulating force transmission between the actin cytoskeleton and focal adhesion proteins.

KEY WORDS: Vinculin, Focal adhesion, Mechanotransduction, Tyrosine phosphorylation, Cell stiffness, Traction, FRAP, Actin pulldown

INTRODUCTION

Adherent cells are anchored through focal adhesions to the extracellular matrix (ECM), which is essential for force transduction, cell spreading and migration (Choquet et al., 1997; Beningo et al., 2001; Bershadsky et al., 2006). Focal adhesions consist of clusters of transmembrane adhesion proteins of the integrin family (Damsky et al., 1985; Gallant et al., 2005; Kanchanawong et al., 2010) and numerous intracellular proteins including α-actinin and talin (Harburger and Calderwood, 2009). Talin links integrins to actin filaments, a bond which is further stabilized by vinculin. The focal adhesion protein vinculin is therefore a key player in building up a strong physical connection for transmitting forces between the cytoskeleton and the ECM (Goldmann et al., 1995, 1996, 1998; Ezzell et al., 1997).

Vinculin consists of an N-terminal globular head and a C-terminal helical tail domain, linked by a flexible proline-rich neck region (Winkler et al., 1996; Ziegler et al., 2006). In the cytoplasm, vinculin exhibits an auto-inhibitory head-to-tail interaction. When it is recruited to focal adhesion sites, vinculin undergoes a conformational change to an open and active state (Johnson and Craig, 1995; Cohen et al., 2005). Various factors and binding partners are thought to be involved in this tightly regulated activation process, including binding of talin or α-actinin to the vinculin head domain, and binding of lipid membranes [e.g. phosphatidylinositol 4,5-bisphosphate (PIP_2)] or actin to the tail domain (Bakolitsa et al., 2004; Izard et al., 2004; Bois et al., 2006; Chen et al., 2006; Janssen et al., 2006; Diez et al., 2009; Peng et al., 2012). Mechanical forces are also thought to stabilize the active state of vinculin (Dumbauld et al., 2013), and external forces applied to the cell increase the recruitment of vinculin and the maturation of focal adhesions (Riveline et al., 2001).

Furthermore, vinculin is assumed to be activated and regulated by phosphorylation of tyrosine residues at positions 100 (in the head), 822 (in the hinge region) and 1065 (in the tail) (Jockusch and Rüdiger, 1996; Zhang et al., 2004). Phosphorylation at position 822 by the kinase Abl is only required for E-cadherin-mediated force transmission and signaling in cell–cell contacts (Subauste et al., 2004), but not for force transmission through cell–ECM adhesions (Bays et al., 2014). By contrast, phosphorylation of vinculin at position 100 and 1065 by Src kinase affects cell spreading and wound repair (Zhang et al., 2004; Moese et al., 2007). Phosphorylation at position 1065 is also associated with the lipid membrane interaction of the vinculin tail domain (Ito et al., 1983; Chandrasekar et al., 2005) and generation of cellular tractions (Diez et al., 2009; Küpper et al., 2010). Recent data have shown that phosphorylation of Y1065 is required for force generation in airway smooth muscle cells during contractile stimulation (Huang et al., 2011, 2014). In addition, molecular dynamics simulations suggest that phosphorylation of Y100 and Y1065 favors the open and active conformation of vinculin (Golji et al., 2012), and more recently it has been shown that phosphorylation of the vinculin tail prevents its binding to vinculin head fragments (Tolbert et al., 2014). Moreover, the same study has demonstrated that a phospho-mimicking mutation at position 1065 does not change the actin co-sedimentation of the full-length protein and has also suggested that phosphorylation of Y1065 does not modulate the binding to actin, but instead alters the bundling of actin filaments through some other mechanism (Tolbert et al., 2014).

Taken together, these results suggest that the lack of phosphorylation renders the vinculin molecule in an inactive conformation and reduces vinculin binding to talin (Diez et al., 2011). However, it remains controversial whether tyrosine phosphorylation at both the positions Y100 and Y1065 is required

[1]Department of Physics, Biophysics Group, University of Erlangen-Nuremberg, 91052 Erlangen, Germany. [2]Institute of Medical Biotechnology, Department of Chemical and Biological Engineering University of Erlangen-Nuremberg, 91052 Erlangen, Germany.

*Author for correspondence (wgoldmann@biomed.uni-erlangen.de)

Received 23 March 2015; Accepted 27 July 2015

Journal of Cell Science (2015) 128, 3435-3443 doi:10.1242/jcs.172031

for vinculin function in cellular force generation and adhesion to the ECM, and whether phosphorylation regulates these parameters by contributing to the conformational activation of vinculin or solely through other mechanisms that include talin and actin binding.

To explore how phosphorylation of the vinculin head (Y100) and/or tail domain (Y1065) affects the protein conformation and thereby the actin-binding affinity, exchange dynamics in focal adhesions and force transmission to the ECM, we analyzed phospho-mimicking and non-phosphorylatable vinculin mutants. These single or double tyrosine mutants were compared to constitutively active (T12) and inactive (A50I) vinculin conformations in mouse embryonic fibroblasts (MEFs) (Table 1). Using traction microscopy, magnetic tweezer microrheology, fluorescence recovery after photobleaching (FRAP) and actin-binding assays, we demonstrate that vinculin phosphorylation of both tyrosine positions is necessary for the conformational activation of vinculin. Thus, phosphorylation together with concomitant protein binding is essential for the regulation of focal adhesions and the transmission of cellular mechanical forces between the actin cytoskeleton, focal adhesions and the ECM.

RESULTS

Phosphorylation and the actin-binding capacity of vinculin define force transmission to the ECM

Vinculin acts as a mechanical coupler between the actin cytoskeleton and the ECM (Ezzell et al., 1997). Previous studies have indicated that the conformational switch from the inactive to active vinculin state is important for force transmission (Diez et al., 2011). To determine the influence of vinculin phosphorylation at the contractile forces of the cells, we used 2D traction microscopy (Fig. 1). MEF vinculin-knockout (KO) cells transfected with different vinculin constructs were seeded on polyacrylamide (PAA) traction gels (Fig. 1A). From the displacement of embedded beads, the exerted forces on the gel surface were calculated (Fig. 1B; supplementary material Fig. S1). As previously shown, vinculin-KO cells generated significantly lower forces on 2D gels than wild-type cells (Mierke et al., 2010). Transfecting knockout cells with full-length vinculin cDNA rescued the force of the knockout cells to the level seen in wild-type cells (Fig. 1C). The constitutively closed protein conformation of the A50I mutant led to a decrease in strain energy, down to one third of the rescue cell level (Diez et al., 2011), whereas the exerted forces of the constitutively open conformation of the T12 mutant were close to wild-type level. Compared to wild-type cells and the T12 mutant, the open vinculin conformation of the Δex20 mutant showed decreased strain energy values because the connection to the actin cytoskeleton would be partially lost. We measured a clear decrease of the exerted cell forces on the substrate when vinculin was non-phosphorylatable. The strain energy values were significantly reduced for Y100F and Y1065F mutants individually as well as for the double mutant Y100F/Y1065F. The vinculin mutants where tyrosine residues had been replaced by glutamic acid (E), mimicking constitutive phosphorylation, showed slightly increased cellular tractions compared to rescue cells. Taken together, these data demonstrate that phosphorylation at both positions 100 and 1065 is necessary for establishing the mechano-coupling function of vinculin and, hence, for force transmission.

Phosphorylation of vinculin changes cellular stiffness and binding strength

Cell stiffness has been shown to scale with the contractile cytoskeletal pre-stress (Wang et al., 2002; Kollmannsberger et al., 2011), and we therefore would expect that the stiffness of the vinculin mutant cells would mirror the traction results reported above. Defined forces were applied to magnetic beads bound to the cell surface through a fibronectin–integrin connection. From the displacement of the bead, we calculated the stiffness of the cell (Fig. 2A–C). Comparing the different vinculin conformational constructs (supplementary material Fig. S2A), the open vinculin conformation of the mutant T12 led to a cell stiffness that was comparable to wild-type cells (Fig. 2D). In contrast, the closed conformation of vinculin A50I mutant reduced cell stiffness to nearly the level of vinculin-KO cells (Diez et al., 2011). Δex20 mutant cells, where vinculin is in its open conformation but devoid of actin-binding, were significantly stiffer than the knockout cells and A50I mutants, but considerably softer than rescue and wild-type cells or cells expressing the constitutively open vinculin mutant T12. The low stiffness values over all force steps of the magnetic tweezer for cells with tyrosine mutations Y100F and/or Y1065F revealed that phosphorylation of vinculin also has a strong influence on cell stiffness (supplementary material Fig. S2B). The cell stiffness of non-phosphorylatable double mutant Y100F/Y1065F decreased to almost the level of the vinculin-KO cells (Fig. 2D).

Table 1. Overview table of vinculin mutants

	Mutation sites			
Vinculin mutant	Head domain (amino acids 1–835)	Tail domain (amino acids 898–1066)	Protein characteristics	References
T12	–	D974A, K975A, R976A, R978A	Open conformation	Cohen et al., 2005; Marg et al., 2010
Δex20	–	Deletion G916–Q983	Open conformation; actin-binding deficient	Marg et al., 2010
A50I	A50I	–	Closed conformation	Bakolitsa et al., 2004; Diez et al., 2011
Y100E	Y100E	–	Phospho-mimicking (open conformation?)	Zhang et al., 2004; Goljiet al., 2012
Y1065E	–	Y1065E	Phospho-mimicking (open conformation?)	Huang et al., 2014; Küpper et al., 2010
Y100E/Y1065E	Y100E	Y1065E	Phospho-mimicking (open conformation?)	Zhang et al., 2004
Y100F	Y100F	–	Non-phosphorylatable (closed conformation?)	Zhang et al., 2004
Y1065F	–	Y1065F	Non-phosphorylatable (closed conformation?)	Tolbert et al., 2014; Diez et al., 2009
Y100F/Y1065F	Y100F	Y1065F	Non-phosphorylatable (closed conformation?)	Moese et al., 2007

Journal of Cell Science

Journal of Cell Science (2015) 128, 3435-3443 doi:10.1242/jcs.172031

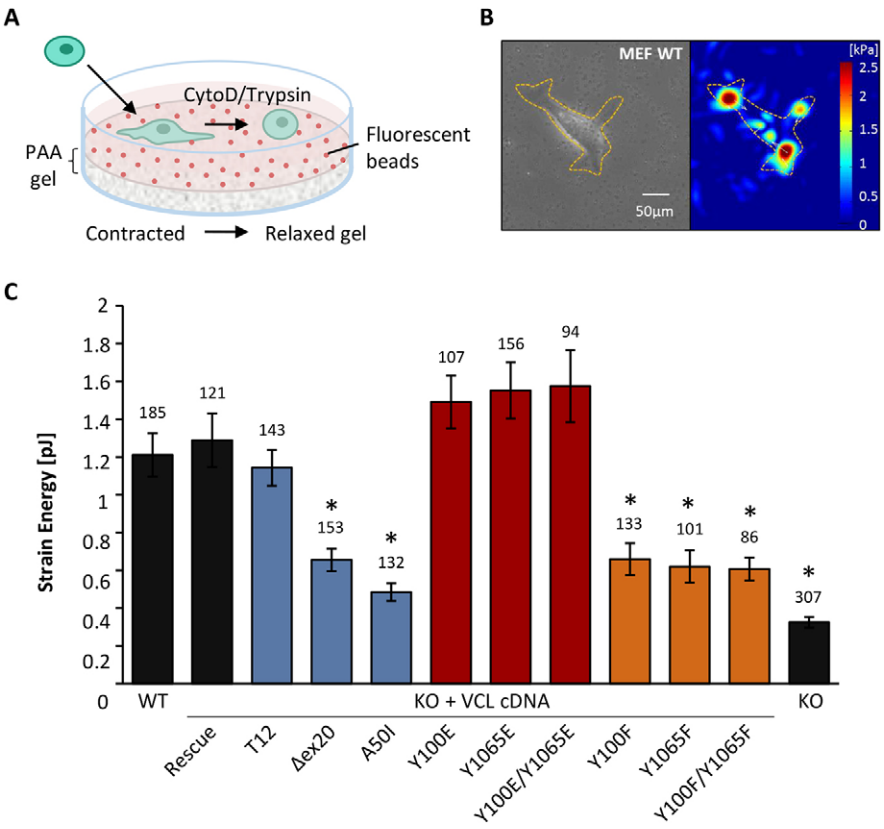

Fig. 1. Measurements of contractile forces by 2D traction microscopy. (A) Schematic representation of the 2D traction setup. Cells attach to fibronectin-coated PAA gels with embedded fluorescent beads. The cells are detached by using cytochalasin D and trypsin, and the elastic gel relaxes to its original position. The bead positions are recorded before and after the relaxation, and tractions forces are calculated from the displacement. (B) A bright-field image (left) and corresponding force map (right) of a wild-type (WT) MEF cell on a PAA gel. The dashed lines outline the cell. The color bar indicates tractions in kPa. Scale bar: 50 µm. (C) Strain energy values are shown for cells expressing vinculin conformational mutants (blue), vinculin phospho-mimicking (red), non-phosphorylatable mutants (orange), and vinculin WT, rescue and KO cells (black). Contractile forces are reduced for impaired actin-binding capacity (Δex20), the inactive conformation (A50I) and after inhibition of phosphorylation (Y100F, Y1065F, Y100F/Y1065F) of the vinculin molecule. Results are means±s.e.m.; the number of analyzed cells is shown above each column. *$P \leq 0.05$ compared to rescue cells (Mann–Whitney U-test).

We measured the stability of the focal adhesion–integrin–fibronectin linkage of the vinculin mutants by examining the percentage of beads that detached during tweezer measurements (Fig. 2E). At an applied force of 10 nN, ~12% of the beads detached from wild-type, rescue and constitutively active vinculin (T12) cells (supplementary material Fig. S2C). The number of detached beads was slightly higher for the Δex20 mutant (~18%) and increased to ~30% for A50I mutant and vinculin-KO cells (supplementary material Fig. S2C). The stability of the connection is also influenced by phosphorylation of vinculin. The percentage of detached beads was significantly higher in non-phosphorylatable (Y100F, Y1065F and Y100F/Y1065F) compared to phospho-mimicking mutants (Y100E, Y1065E, Y100E/Y1065E) (Fig. 2E; supplementary material Fig. S2D). These measurements provide further evidence of the mechanical importance of vinculin phosphorylation.

Vinculin dynamics at focal adhesions depends on protein conformation and phosphorylation

The results from mechanical measurements showed that traction forces and stiffness of non-phosphorylatable vinculin mutants are comparable to those of mutants with inactive (closed conformation) vinculin. To determine whether phosphorylation-induced conformational changes influence the binding affinity of vinculin to focal adhesion proteins, FRAP assays of different eGFP-tagged vinculin mutants were performed (Fig. 3A). MEF knockout cells rescued by wild-type vinculin showed a half-life recovery time ($T_{1/2}$) of about 67 s, whereas the closed A50I conformation of vinculin showed a clear decrease in recovery time to ~21 s (Fig. 3B, C). By contrast, the recovery times of the vinculin mutant T12 were three-fold higher compared to rescue cells. The recovery time in the vinculin mutant Δex20 was faster compared to the T12 mutant, but slower than in rescue cells (Marg et al., 2010). These findings are in accordance with reports that vinculin in its active, open conformation binds more stably to focal adhesions, displaying slower exchange dynamics (Cohen et al., 2006). We next compared these known vinculin conformations with tyrosine mutants to examine the influence of phosphorylation on the protein conformation (Fig. 3C). FRAP data revealed that the phospho-mimicking mutants did not increase the recovery time significantly. However, the inhibition of phosphorylation either in the head (Y100F) or in the tail domain (Y1065F) triggered vinculin mutants to recover much faster after photobleaching, indicating that they are less stably incorporated in focal adhesions, presumably because of a closed vinculin state that could not be fully activated by other binding partners.

From the FRAP curves, we also calculated the mobile and immobile fraction of the protein within focal adhesions. Cells transfected with wild-type vinculin showed a mobile fraction of ~70%, compared to ~50% in T12 mutant cells (Fig. 3D). The immobile fraction was not significantly changed in the Δex20 and A50I mutants. Whereas the non-phosphorylatable vinculin mutants exhibited a similar amount of vinculin in mobile and immobile fractions to rescue cells, the phospho-mimicking Y100E and Y1065E mutants showed increased immobile fractions of vinculin in focal adhesions. Taken together, these data demonstrate that phosphorylation increases the binding strength of vinculin to other focal adhesion proteins (Fig. 3C,D).

Phosphorylation of vinculin facilitates binding of talin and F-actin

Besides the conformational opening of the protein, the actin-binding properties of vinculin are equally crucial for its mechanical function. To test whether tyrosine phosphorylation is needed for vinculin activation and consequently for proper coupling to the actin cytoskeleton, we performed an F-actin co-sedimentation assay with purified wild-type vinculin protein and both double mutants Y100E/Y1065E and Y100F/Y1065F. Fig. 4A shows a

Journal of Cell Science (2015) 128, 3435-3443 doi:10.1242/jcs.172031

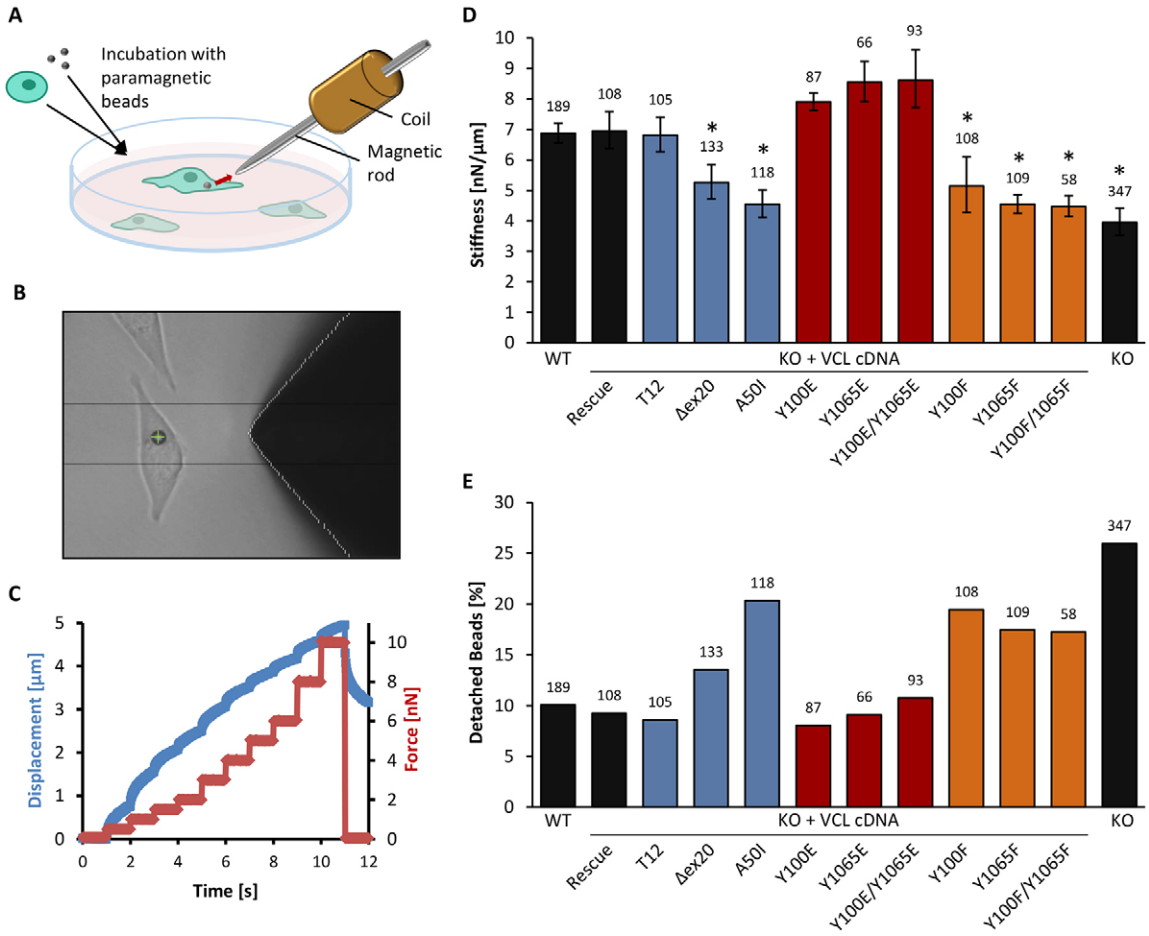

Fig. 2. Cell stiffness and adhesive forces determined by magnetic tweezer experiments. (A) Schematic representation of the magnetic tweezer setup. Cells are seeded overnight on a cell culture dish and incubated with ECM-coated paramagnetic beads 30 min prior to measurements. A magnetic field is applied to the bead attached to integrins, and the displacement of the bead is recorded. (B) Bright-field image of the magnetic tweezer tip close to a tracked magnetic bead (green cross) attached to the cell. (C) Increasing bead displacement (blue) with increasing force steps at 1 nN/s (red). (D) Stiffness values at 6 nN force are shown for cells expressing vinculin conformational (blue), phospho-mimicking (red) and non-phosphorylatable mutants (orange), as well as for vinculin wild-type (WT), rescue and KO cells (black). The cell stiffness decreases significantly for actin-binding deficient (Δex20), inactive (A50I), non-phosphorylatable (Y100F, Y1065F, Y100F/Y1065F) vinculin mutants and KO cells. Phospho-mimicking mutants (Y100E, Y1065E, Y100E/Y1065E) show slightly higher values than WT, rescue and T12 cells. (E) The percentage of detached beads at 6 nN force was increased for the vinculin mutants Δex20, A50I, Y100F, Y1065F, Y100F/Y1065F and KO cells compared to vinculin WT, rescue, T12 and phospho-mimicking mutants. Results are means±s.e.m.; the number of analyzed cells is shown above each column. *$P \leq 0.05$ compared to rescue cells (Mann–Whitney U-test).

representative SDS-PAGE gel. After incubation with actin and ultracentrifugation, only ∼10% of vinculin had co-sedimented with actin (Fig. 4A,C), regardless of the mutation. When we supported the activation of the vinculin molecule by adding a peptide containing the third vinculin-binding site from talin (VBS3) at a saturating high concentration (200 µM), the percentage of vinculin in the pellet fraction increased to ∼50% (supplementary material Fig. S3), again regardless of the mutation (Fig. 4B,C), which is in agreement with published data (Bass et al., 2002). However, at low VBS3 concentrations (5 µM), large differences between the vinculin mutants appeared: the pellet fraction of non-phosphorylated wild-type and non-phosphorylatable Y100F/Y1065F vinculin contained ∼20% of the protein, whereas it was ∼50%, and thus reached saturation level, in the phospho-mimicking mutant Y100E/Y1065E, indicating a higher sensitivity for the activating effect of VBS3 and a stronger binding of this vinculin mutant with F-actin (Fig. 4A,C). This result supports the hypothesis that phosphorylation facilitates protein activation and enhances the accessibility of actin-binding sites on vinculin.

DISCUSSION

Vinculin is an auto-inhibited molecule that is present in the cytoplasm in a closed, inactive conformation. By a number of different mechanisms that are currently not completely understood, the vinculin molecule can switch from an inactive, closed conformation to an open, active conformation, which exposes binding sites for cytoskeletal and focal adhesion proteins, most importantly for actin and talin. Among the mechanisms that are thought to activate vinculin are binding of the vinculin head to talin, binding of the vinculin tail to actin, membrane interactions (e.g. through PIP_2) and phosphorylation of vinculin (Ziegler et al., 2006; Goldmann et al., 2013). Once activated, the binding of vinculin to actin and talin is stabilized, and through this coupling, mechanical forces are transmitted to the ECM (Thievessen et al., 2013). These mechanical forces are believed to keep the vinculin molecule in its open, active conformation (Grashoff et al., 2010).

In this study, we demonstrate that Src-mediated phosphorylation of vinculin at position 100 (head domain) and at position 1065 (tail domain) are both required for vinculin activation and for mechanical

Journal of Cell Science (2015) 128, 3435-3443 doi:10.1242/jcs.172031

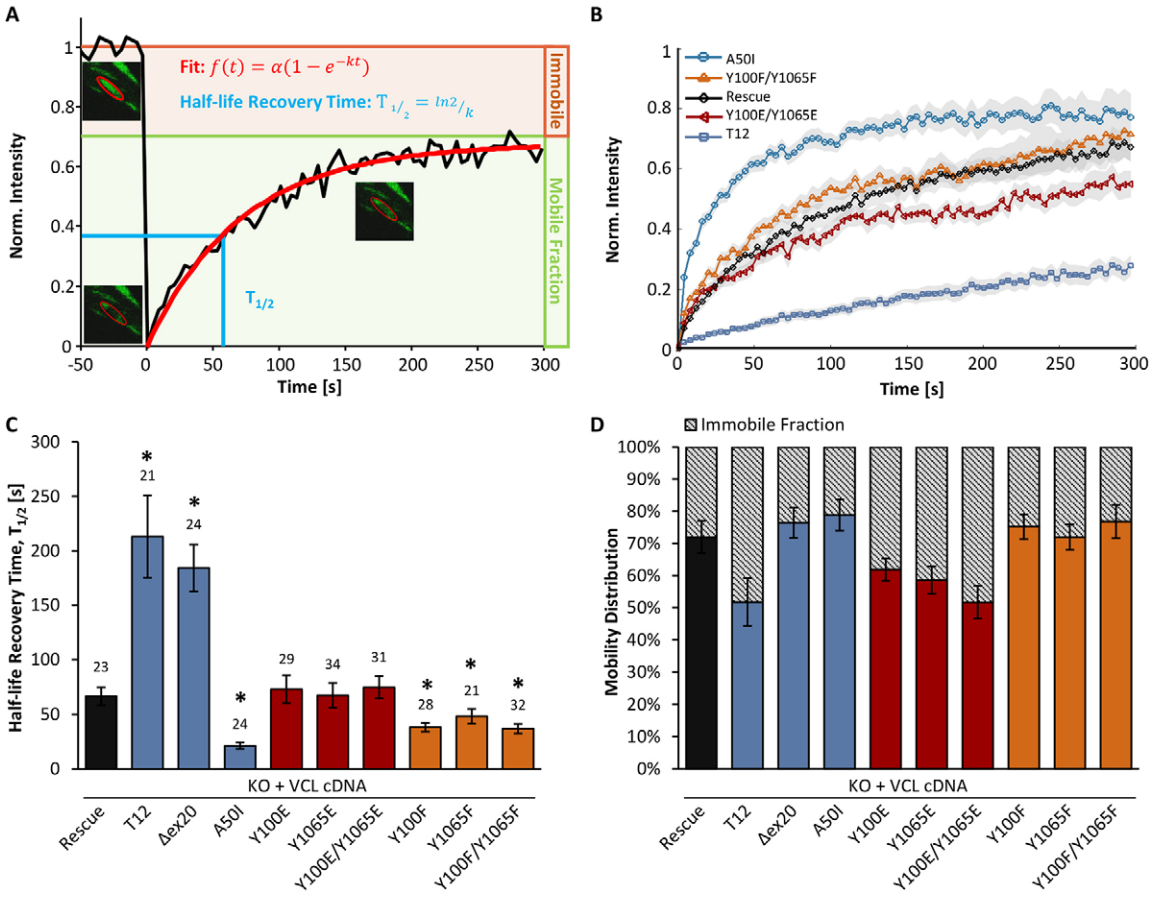

Fig. 3. Fluorescence recovery after photobleaching (FRAP) of different vinculin mutants. (A) Recovery curve of a bleached vinculin rescue cell. Intensity of the bleached area is plotted over time, and the single exponential fit is shown in red. Images of the bleached focal adhesion are shown at *t*=−4 s, *t*=0 s and *t*=160 s. (B) Fluorescence recovery of different vinculin mutants (rescue, T12, A50I, Y100E/Y1065E, Y100F/Y1065F) after photobleaching (mean, with the s.e.m. shown by the region shaded gray; the number of analyzed cells is shown above each column in C). (C) The half-life recovery time, $T_{1/2}$ is significantly increased for the active, open conformations T12 and Δex20 and decreased for the inactive, closed (A50I), and non-phosphorylatable vinculin (Y100F, Y1065F, Y100F/Y1065F) mutants and KO cells compared to rescue cells and phospho-mimicking (Y100E, Y1065E, Y100E/Y1065E) mutants. (D) The mobility distribution shows the percentage of mobile and immobile vinculin proteins in focal adhesions. The immobile fraction is increased for T12 and phospho-mimicking mutants (Y100E, Y1065E, Y100E/Y1065E) compared to rescue cells and Δex20, A50I, Y100F, Y1065F and Y100F/Y1065F mutants. Results are means±s.e.m.; the number of analyzed cells is shown above each column in C. **P*≤0.05 compared to rescue cells (Mann–Whitney U-test).

force transmission across focal adhesions. Using 2D traction microscopy and magnetic tweezer microrheology with beads coupled to integrin receptors, we determined cellular contractile forces, stiffness and binding strength. We also analyzed the exchange dynamics of vinculin in focal adhesions by FRAP, and the binding interaction of purified vinculin to actin by co-sedimentation assays.

To address whether Src-mediated phosphorylation induces conformational changes in the vinculin molecule and increases its affinity for binding partners, we used phospho-mimicking (Y100E, Y1065E and Y100E/Y1065E) and non-phosphorylatable (Y100F, Y1065F, Y100F/Y1065F) vinculin mutants. Results from 2D traction microscopy and magnetic tweezer measurements showed a strong reduction of cellular tractions, stiffness and adhesive forces in all non-phosphorylatable vinculin mutants. These data are in agreement with previous reports showing that the non-phosphorylatable double mutant Y100F/Y1065F is not able to rescue the spreading defect in vinculin-KO cells (Zhang et al., 2004; Moese et al., 2007). The exchange dynamics of non-phosphorylatable vinculin in focal adhesions was markedly increased compared to wild-type vinculin, further supporting the notion that non-phosphorylatable vinculin shows impaired binding to other focal adhesion proteins and is therefore not able to transmit mechanical forces.

Phospho-mimicking mutants, by contrast, showed slightly higher cellular tractions, stiffness and adhesive forces than vinculin wild-type cells. The exchange dynamics of phospho-mimicking vinculin in focal adhesions was similar to rescue cells but showed a higher immobile fraction. Taken together, these data demonstrate that tyrosine phosphorylation of vinculin is necessary for force transmission across focal adhesions, which supports the hypothesis that tyrosine phosphorylation is required for an open, active conformation of vinculin.

To test this hypothesis, we analyzed several vinculin mutants with defined conformations: (1) a constitutively inactive, closed molecule (A50I), (2) a constitutively active, open molecule devoid of actin-binding (Δex20), and (3) a constitutively active, open molecule (T12). Vinculin in the closed conformation (A50I) showed impaired force transmission and increased exchange dynamics in focal adhesions (Cohen et al., 2006; Diez et al., 2011), similar to our data obtained with non-phosphorylatable vinculin mutants. Δex20 vinculin also showed impaired force transmission, as expected from the missing actin-binding capacity, and displayed slower exchange dynamics, as expected from its

Journal of Cell Science (2015) 128, 3435-3443 doi:10.1242/jcs.172031

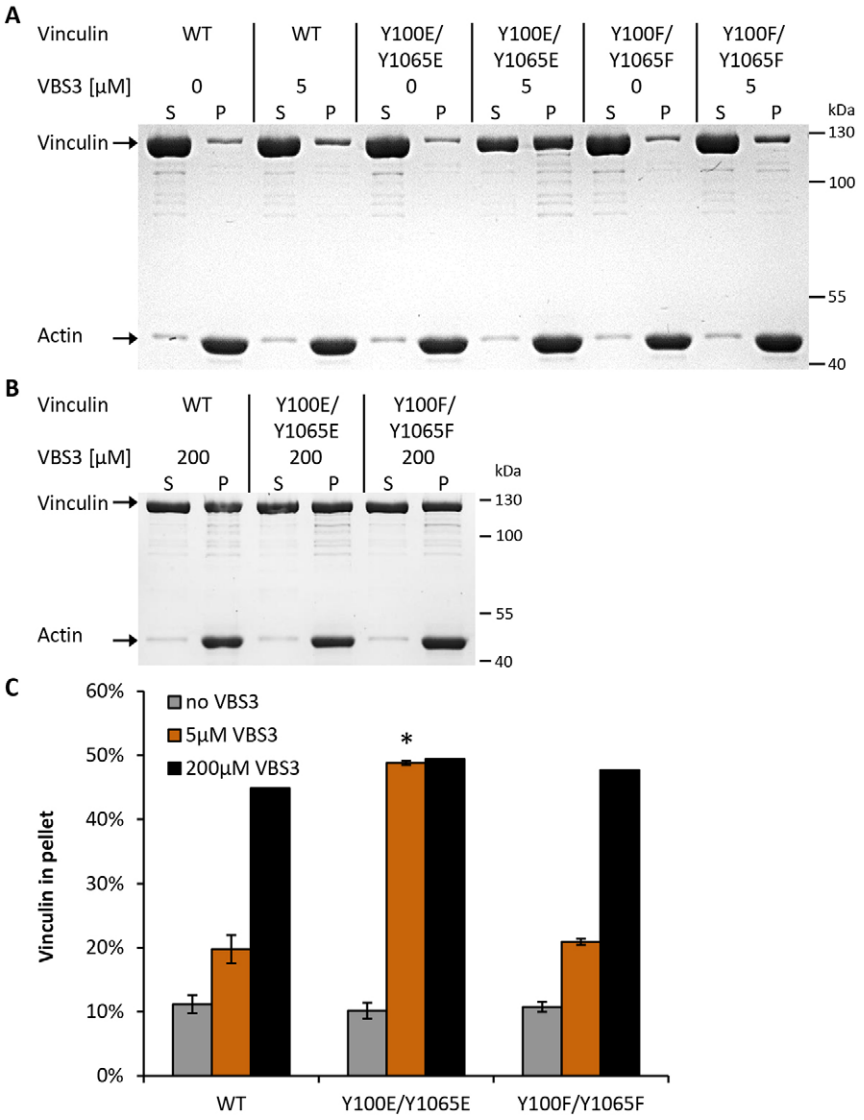

Fig. 4. Co-sedimentation assays of vinculin mutants with F-actin in the presence or absence of VBS3. (A) Purified wild-type (WT) vinculin and the indicated vinculin mutants were incubated with F-actin in the presence or absence of 5 µM VBS3. After ultracentrifugation, the supernatant (S) and pellet (P) fractions were separated, and the amount of proteins was analyzed by SDS-PAGE. The amount of vinculin in the pellet fraction only increased for the Y100E/Y1065E mutant. (B) Co-sedimentation of vinculin with F-actin in the presence of 200 µM VBS3. (C) The graph shows the percentage of vinculin in the pellet for all mutants under three different conditions (0 µM VBS3 in gray, 5 µM VBS3 in orange and 200 µM VBS3 in black) after quantitative analysis of the protein bands (n=3). Without VBS3, ~10% of vinculin co-sedimented with F-actin. Using 5 µM VBS3, the co-sedimentation of WT and Y100F/Y1065F mutant with F-actin increased to 20% and for Y100E/Y1065E mutant up to 50%. Using 200 µM VBS3, all vinculin proteins co-sedimented with F-actin to similar levels (~50%). Results are means±s.e.m. *P≤0.05 compared to rescue cells (Mann–Whitney U-test).

constitutively open conformation (Marg et al., 2010). Constitutively active T12 mutants also displayed slower exchange dynamics in focal adhesions but a similarly increased immobile fraction compared to phospho-mimicking vinculin (Cohen et al., 2006; Humphries et al., 2007). Interestingly, the force transmission in T12 mutants, in phospho-mimicking vinculin mutants and in rescue cells was similar, suggesting that the vinculin present in the focal adhesions of wild-type cells is mostly in an open, active conformation, which is in agreement with data from FRET-based experiments (Chen et al., 2005).

Taken together, the comparison of the biomechanical signatures of vinculin phospho-mutants with those of vinculin mutants with known conformations suggests that tyrosine phosphorylation is necessary for an open, active conformation of vinculin. This finding is also supported by a recent FRET-based study describing that Y1065E vinculin molecules that are recruited to the membrane in smooth muscle cells after acetylcholine stimulation become activated, whereas Y1065F molecules remain in a closed conformation (Huang et al., 2014).

However, the lower exchange dynamics of the constitutively open T12 and Δex20 mutants compared to our phospho-mimicking mutants suggest that phosphorylation alone is not sufficient for vinculin activation. Indeed, previous experiments have demonstrated that phospho-mimicking vinculin failed to co-sediment with actin filaments in pulldown assays (Zhang et al., 2004; Tolbert et al., 2014).

Numerous studies have claimed that talin or other binding partners must be present for vinculin to become activated (Bakolitsa et al., 2004; Izard and Vonrhein, 2004; Bois et al., 2006). It has been hypothesized that vinculin phosphorylation facilitates this activation by increasing the intramolecular distance between the vinculin head and tail (Golji et al., 2011; Auernheimer and Goldmann, 2014). We therefore investigated whether phosphorylation by the Src kinase creates conditions that enable binding partners to activate vinculin. As a binding partner, we used a peptide containing VBS3. This talin fragment has been shown to activate and open the vinculin molecule by binding in the head region (Bass et al., 2002). High concentrations of VBS3 (200 µM) strongly increased the fraction of vinculin that co-sedimented with F-actin, but under these saturated conditions, we detected no difference between the phospho-mimicking (Y100E/Y1065E) and non-phosphorylated proteins (wild-type and Y100F/Y1065F). However, when the concentration of VBS3 was lowered to 5 µM, we observed large differences. The co-sedimentation of phospho-mimicking vinculin was strongly (fivefold) increased and reached saturation levels, whereas the co-sedimentation of the non-

Journal of Cell Science (2015) 128, 3435-3443 doi:10.1242/jcs.172031

phosphorylated mutants was only increased twofold compared to the reaction without the VBS3 peptide. These data reveal that phosphorylated vinculin can be activated more readily in the presence of a binding partner such as talin, which results in an open conformation, exposing the actin binding-sites. Therefore, the actin binding assays support the hypothesis that phosphorylation is a prerequisite for vinculin activation.

Taken together, our data demonstrate that tyrosine phosphorylation of vinculin plays a pivotal role for cellular mechanics and force transmission in focal adhesions, and that phosphorylation of both Y100 and Y1065 is necessary to fully activate the vinculin molecule. As a possible mechanism, we consider that phosphorylation of vinculin takes place in two steps, with distinct functions of the two Src phosphorylation sites (Y100 and Y1065). The tyrosine residue on position 100 is described as fully accessible in the three-dimensional structure of the closed protein conformation, whereas positon 1065 is hidden by sequences of the proline-rich linker region (Bakolitsa et al., 2004). In addition, molecular dynamics simulations have shown that position 1065 does not directly influence the auto-inhibiting interaction of the vinculin head and tail domain (Golji et al., 2012). Thus, the main contribution of Y1065 is to stabilize the interaction between F-actin and the vinculin tail and possibly to facilitate actin bundling (Tolbert et al., 2014), whereas Y100 is thought to be responsible for the conformational activation. In the first step, the phosphorylation of the accessible Y100 in the head domain elicits a conformational rearrangement of the protein that facilitates the subsequent phosphorylation of Y1065 by Src. This second phosphorylation might further stabilize or augment the conformational activation, as *in vitro* binding assays of isolated head fragments display a decreased level of interaction with non-phosphorylated tail fragments (Zhang et al., 2004). Therefore, Src-mediated phosphorylation at both residues is required for the concomitant binding of talin to the vinculin head domain and of actin to the vinculin tail domain, which in turn is a prerequisite for force transmission. Phosphorylation and de-phosphorylation of vinculin might be a plausible mechanism explaining how the remodeling, assembly and disassembly of focal adhesions are regulated to control dynamic cell behavior and cell migration.

MATERIALS AND METHODS

Cell lines

Wild-type and vinculin-KO MEFs were obtained from Dr W. H. Ziegler (University of Leipzig, Leipzig, Germany) (Mierke et al., 2010). MEFs were cultured in low-glucose (1 g/l) Dulbecco's modified Eagle's medium (Gibco) supplemented with 10% fetal calf serum (Sigma-Aldrich) and 2 mM L-glutamine (Invitrogen) at 37°C with 5% CO_2. Mycoplasma contamination was prevented by using a mycoplasma detection kit (Minerva Biolabs).

Vinculin mutants

Vinculin mutants of different conformations, actin-binding properties or phosphorylation states were used to analyze the function of vinculin (Table 1). Full-length eGFP-tagged vinculin cDNA was expressed in vinculin-KO MEFs to rescue the wild-type phenotype. A constitutively open protein conformation was tested using the mutant T12, which contains four point mutations in the tail domain (D974A, K975A, R976A and R978A) that inhibit the intramolecular head-to-tail interaction (Cohen et al., 2005). Another open conformation was the Δex20 mutant, which lacks amino acids 916–983 of the exon 20 (Marg et al., 2010). This deletion disrupts the autoinhibition of vinculin and additionally inhibits the binding to the actin cytoskeleton because the actin-binding sites are localized within the deleted region of exon 20. The effect of a constitutively closed vinculin protein was investigated with the mutant A50I (Bakolitsa et al., 2004). This point mutation in the head domain blocks the interaction with talin. To analyze the effect of tyrosine phosphorylation, Y100 and Y1065 were replaced by phenylalanine residues to inhibit phosphorylation at the respective sides (Y100F, Y1065F and Y100F/Y1065F) or by glutamic acid to mimic permanent phosphorylation (Y100E, Y1065E and Y100E/Y1065E). The point mutations are located in the vinculin head (Y100) or in the tail domain (Y1065).

Mutagenesis and transfection of vinculin cDNA

Vinculin mutants T12 and Δex20 were kindly provided by Dr W. H. Ziegler (University of Leipzig, Leipzig, Germany). Generation of the eukaryotic expression vector pcDNA3.1 containing eGFP-tagged wild-type vinculin or the A50I vinculin mutant, has been described previously (Diez et al., 2009, 2011). The same cDNA vector was used to create the tyrosine mutants by site-directed mutagenesis, replacing Y100 and Y1065 with phenylalanine or glutamic acid residues.

The point mutations were induced using primers from Eurofins MWG Operon, Phusion High-Fidelity DNA Polymerase, and the restriction enzyme DpnI (New England Biolabs) for the digestion of methylated DNA. Expression vectors were amplified in the *Escherichia coli* strain Dh5α and purified using the NucleoBond PC 500 kit (Macherey-Nagel). The complete sequence for all GFP-tagged vinculin mutants was confirmed by sequencing (GATC Biotech AG).

MEFs (1.5×10^5) were seeded overnight in 35-mm cell culture dishes prior to transfection. Transfection was carried out in serum-free DMEM using 2 µg DNA and Lipofectamine 2000 (Invitrogen). The day after transfection, cells were re-seeded in a 35-mm culture dish or on PAA traction gels, respectively.

Vinculin expression and purification

Vinculin cDNA and the vinculin constructs Y100E/Y1065E and Y100F/Y1065F were cloned into a pET28a expression vector and expressed in BL21-CodonPlus® (DE3)-RIL as follows. Bacteria were grown in LB medium supplemented with chloramphenicol and kanamycin at 37°C to an optical density at 600 nm (OD_{600nm}) of 0.6. Expression of the recombinant proteins was induced with 0.5 mM isopropyl β-D-1-thiogalactopyranoside. Cultures were grown overnight (16 h) at 18°C. Bacteria were pelleted and resuspended in lysis buffer (50 mM Tris-HCl pH 8.0, 500 mM NaCl, 10 mM imidazole, 5 mM β-mercaptoethanol, 1 mg/ml lysozyme, 0.1 mg/ml DNase, 1 mM phenylmethane-sulfonylfluoride and 1 mM benzamidine) and sonicated. The supernatant of the clarified lysate [20,217 ***g*** (14,000 rpm), 15 min, 4°C] was loaded on a Ni-chelate column (Qiagen), washed with 10 mM imidazole in 50 mM Tris-HCl pH 8.0, 500 mM NaCl and 5 mM β-mercaptoethanol, and vinculin was eluted with 250 mM imidazole in 50 mM Tris-HCl pH 8.0, 500 mM NaCl, and 5 mM β-mercaptoethanol. For further purification, anion exchange columns (HiTrap Q HP and Mono Q, GE Healthcare) were used. The eluted protein was concentrated using YM-50 centricons (Millipore). Purity and concentration of all vinculin proteins were evaluated by SDS-PAGE prior to use.

2D-traction microscopy

This technique measures the forces that cells exert on their surroundings by observing the displacements of beads embedded in a flexible gel substrate on which the cells are cultured. Elastic polyacrylamide (PAA) hydrogels with embedded red fluorescent beads were prepared as described previously (Pelham and Wang, 1997). Acrylamide-bisacrylamide (29:1, Sigma-Aldrich) gels of 7% have a Young's modulus of ∼18 kPa. The surface of the gel was activated using Sulfo-SANPHA (Thermo Fisher Scientific) under UV light for 5 min and coated with fibronectin (Roche). Cells were seeded 24 h before measurements and cultured at 37°C, 5% CO_2, and 95% humidity. Bright field as well as fluorescence (red and green channel) images of adhered cells and the deformed gel were taken with an inverted microscope (DMI Leica). Using 16 µM cytochalasin D and 0.07% trypsin, cells were relaxed and detached. Images were recorded of the relaxed undeformed gel. Bead displacements due to cell tractions were quantified by image flow velocimetry, and cell tractions were computed using the Fourier

transform traction cytometry method (Butler et al., 2002). From the displacement field and the traction force, the strain energy was calculated.

Magnetic tweezer microrheology

Using the magnetic tweezer, mechanical shear stress is exerted to the cell by applying lateral forces to magnetic beads that are connected to the cytoskeleton through adhesion contacts (integrins) on the apical cell surface. This method reports the passive mechanical properties of the cytoskeleton, such as the elastic modulus and its time dependency (Kollmannsberger and Fabry, 2007; Fabry et al., 2011). In brief, the magnetic tweezer is attached to an inverted microscope (DMI Leica, 40×, 0.6 NA objective). The device consists of a solenoid with 250 turns of 0.4 mm diameter copper wire around a high-permeability, μ-metal core with a thin pointed tip.

MEFs (3×10^4) were seeded in 35-mm culture dishes the day before experiments and incubated with fibronectin-coated 4.5 μm epoxylated superparamagnetic beads (Invitrogen) 30 min before measurements. Cells were checked for correctly bound beads, and in case of transfected cells, for eGFP expression, before magnetic pulling forces were applied. A staircase-like increasing force was then used for 10 s to the bead bound on the cell surface (Alenghat et al., 2000; Mierke et al., 2008). Images were recorded by a CCD-camera (ORCA ER, Hamamatsu) at a rate of 40 frames/s, and the resulting bead displacement d(t) was calculated from the tracked positions with a center-of-mass algorithm (Hildebrandt, 1969; Fabry et al., 2001; Kasza et al., 2009; Kollmannsberger et al., 2011). The creep response J(t) of the cells follows a power law with time, $J(t)=J_0(t/t_0)^b$. The parameter J_0 (μm/nN) is the creep compliance at t_0 and corresponds to the inverse magnitude of the dynamic shear modulus of the cells (stiffness) (Mierke et al., 2008). During force application to 10 nN, we additionally recorded the lowest force step of bead detachment. The percentage of detached beads related to the corresponding force was used to quantify the binding (adhesion) strength of the cell surface receptors.

Fluorescence recovery after photobleaching

FRAP assays were performed with the confocal microscope (Leica) and a 20× dip-in objective inside the incubation chamber. Transfected cells were cultivated in 35-mm dishes the day before experiments, and cells expressing medium levels of eGFP–vinculin constructs and with focal adhesions showing no growth or disassembly, were chosen for measurements. A 488-nm argon laser was used for eGFP excitation and bleaching. Image acquisition started 1 min before bleaching and continued for 5 min of the recovery process (1 frame every 4 s). FRAP movies were analyzed using ImageJ and Matlab software. Average intensities of the bleached focal adhesion as well as reference adhesions were corrected for background fluorescence and subsequently the bleached area was normalized by the reference adhesion signal. Every recovery curve was fitted using a single exponential function, and the mean value of half-life recovery times ($T_{1/2}$) was calculated (Fig. 3A).

Actin co-sedimentation assays

The actin-binding capacity of phospho-mimicking and non-phosphorylatable vinculin mutants was determined using an actin protein binding kit (Cytoskeleton). To support the activation of vinculin, a 26-amino-acid long sequence from the vinculin-binding partner talin, the vinculin-binding site 3 (VBS3; YTKKELIESARKVSEKVSHVLAALQA) was synthesized (Biomatik) and added to the reaction. Polymerized F-actin (9.5 μM) was incubated with purified vinculin protein (3.8 μM) and various concentrations of VBS3 peptide (0–200 μM) for 1 h at room temperature. Preliminary experiments showed that co-sedimentation of vinculin with F-actin saturates at a concentration of 200 μM VBS3. Samples of 100 μl were centrifuged at 100,000 ***g*** for 1 h at 4°C. The supernatant was separated, and the pellet was resuspended in 100 μl water. Samples were analyzed by SDS-PAGE. The Coomassie-stained gels were densitometrically quantified using ImageJ software, and the percentage of total vinculin protein in the pellet fraction was calculated.

Acknowledgements

We thank Dr Ingo Thievessen for helpful discussions.

Competing interests

The authors declare no competing or financial interests.

Author contributions

V.A. and W.H.G. developed the concept and designed the study. V.A., L.A.L., M.L., and B.K. performed and analyzed the experiments. B.F. and O.F. developed the methods. V.A., B.K., B.F., and W.H.G. wrote the manuscript.

Funding

This work was supported by grants from Deutscher Akademischer Austauschdienst (DAAD) [grant number 50021371 to W.H.G.]; Deutsche Forschungsgemeinschaft (DFG) [grant number FA336-6]; and the National Institutes of Health (NIH) [grant number BRP:HL65960 to B.F.]. Deposited in PMC for release after 12 months.

Supplementary material

Supplementary material available online at
http://jcs.biologists.org/lookup/suppl/doi:10.1242/jcs.172031/-/DC1

References

Alenghat, F. J., Fabry, B., Tsai, K. Y., Goldmann, W. H. and Ingber, D. E. (2000). Analysis of cell mechanics in single vinculin-deficient cells using a magnetic tweezer. *Biochem. Biophys. Res. Commun.* **277**, 93-99.

Auernheimer, V. and Goldmann, W. H. (2014). Serine phosphorylation on position 1033 of vinculin impacts cellular mechanics. *Biochem. Biophys. Res. Commun.* **450**, 1095-1098.

Bakolitsa, C., Cohen, D. M., Bankston, L. A., Bobkov, A. A., Cadwell, G. W., Jennings, L., Critchley, D. R., Craig, S. W. and Liddington, R. C. (2004). Structural basis for vinculin activation at sites of cell adhesion. *Nature* **430**, 583-586.

Bass, M. D., Patel, B., Barsukov, I. G., Fillingham, I. J., Mason, R., Smith, B. J., Bagshaw, C. R. and Critchley, D. R. (2002). Further characterization of the interaction between the cytoskeletal proteins talin and vinculin. *Biochem. J.* **362**, 761-768.

Bays, J. L., Peng, X., Tolbert, C. E., Guilluy, C., Angell, A. E., Pan, Y., Superfine, R., Burridge, K. and DeMali, K. A. (2014). Vinculin phosphorylation differentially regulates mechanotransduction at cell-cell and cell-matrix adhesions. *J. Cell Biol.* **205**, 251-263.

Beningo, K. A., Dembo, M., Kaverina, I., Small, J. V. and Wang, Y.-l. (2001). Nascent focal adhesions are responsible for the generation of strong propulsive forces in migrating fibroblasts. *J. Cell Biol.* **153**, 881-888.

Bershadsky, A. D., Ballestrem, C., Carramusa, L., Zilberman, Y., Gilquin, B., Khochbin, S., Alexandrova, A. Y., Verkhovsky, A. B., Shemesh, T. and Kozlov, M. M. (2006). Assembly and mechanosensory function of focal adhesions: experiments and models. *Eur. J. Cell Biol.* **85**, 165-173.

Bois, P. R. J., O'Hara, B. P., Nietlispach, D., Kirkpatrick, J. and Izard, T. (2006). The vinculin binding sites of talin and alpha-actinin are sufficient to activate vinculin. *J. Biol. Chem.* **281**, 7228-7236.

Butler, J. P., Tolic-Norrelykke, I. M., Fabry, B. and Fredberg, J. J. (2002). Traction fields, moments, and strain energy that cells exert on their surroundings. *Am. J. Physiol. Cell Physiol.* **282**, C595-C605.

Chandrasekar, I., Stradal, T. E. B., Holt, M. R., Entschladen, F., Jockusch, B. M. and Ziegler, W. H. (2005). Vinculin acts as a sensor in lipid regulation of adhesion-site turnover. *J. Cell Sci.* **118**, 1461-1472.

Chen, X., Yang, Y., Wang, F., Chen, Y. and Xia, Y. (2005). Generation and evolution of quadratic dark spatial solitons using the wavefront modulation method. *Opt. Expr.* **13**, 8699-8707.

Chen, H., Choudhury, D. M. and Craig, S. W. (2006). Coincidence of actin filaments and talin is required to activate vinculin. *J. Biol. Chem.* **281**, 40389-40398.

Choquet, D., Felsenfeld, D. P. and Sheetz, M. P. (1997). Extracellular matrix rigidity causes strengthening of integrin–cytoskeleton linkages. *Cell* **88**, 39-48.

Cohen, D. M., Chen, H., Johnson, R. P., Choudhury, B. and Craig, S. W. (2005). Two distinct head-tail interfaces cooperate to suppress activation of vinculin by talin. *J. Biol. Chem.* **280**, 17109-17117.

Cohen, D. M., Kutscher, B., Chen, H., Murphy, D. B. and Craig, S. W. (2006). A conformational switch in vinculin drives formation and dynamics of a talin-vinculin complex at focal adhesions. *J. Biol. Chem.* **281**, 16006-16015.

Damsky, C. H., Knudsen, K. A., Bradley, D., Buck, C. A. and Horwitz, A. F. (1985). Distribution of the cell substratum attachment (CSAT) antigen on myogenic and fibroblastic cells in culture. *J. Cell Biol.* **100**, 1528-1539.

Diez, G., Kollmannsberger, P., Mierke, C. T., Koch, T. M., Vali, H., Fabry, B. and Goldmann, W. H. (2009). Anchorage of vinculin to lipid membranes influences cell mechanical properties. *Biophys. J.* **97**, 3105-3112.

Diez, G., Auernheimer, V., Fabry, B. and Goldmann, W. H. (2011). Head/tail interaction of vinculin influences cell mechanical behavior. *Biochem. Biophys. Res. Commun.* **406**, 85-88.

Dumbauld, D. W., Lee, T. T., Singh, A., Scrimgeour, J., Gersbach, C. A., Zamir, E. A., Fu, J., Chen, C. S., Curtis, J. E., Craig, S. W. et al. (2013). How vinculin regulates force transmission. *Proc. Natl. Acad. Sci. USA* **110**, 9788-9793.
Ezzell, R. M., Goldmann, W. H., Wang, N., Parashurama, N. and Ingber, D. E. (1997). Vinculin promotes cell spreading by mechanically coupling integrins to the cytoskeleton. *Exp. Cell Res.* **231**, 14-26.
Fabry, B., Maksym, G. N., Butler, J. P., Glogauer, M., Navajas, D. and Fredberg, J. J. (2001). Scaling the microrheology of living cells. *Phys. Rev. Lett.* **87**, 148102.
Fabry, B., Klemm, A. H., Kienle, S., Schäffer, T. E. and Goldmann, W. H. (2011). Focal adhesion kinase stabilizes the cytoskeleton. *Biophys. J.* **101**, 2131-2138.
Gallant, N. D., Michael, K. E. and García, A. J. (2005). Cell adhesion strengthening: contributions of adhesive area, integrin binding, and focal adhesion assembly. *Mol. Biol. Cell* **16**, 4329-4340.
Goldmann, W. H. and Ezzell, R. M. (1996). Viscoelasticity in wild-type and vinculin-deficient (5.51) mouse F9 embryonic carcinoma cells examined by atomic force microscopy and rheology. *Exp. Cell Res.* **226**, 234-237.
Goldmann, W. H., Schindl, M., Cardozo, T. J. and Ezzell, R. M. (1995). Motility of vinculin-deficient F9 embryonic carcinoma cells analyzed by video, laser confocal, and reflection interference contrast microscopy. *Exp. Cell Res.* **221**, 311-319.
Goldmann, W. H., Galneder, R., Ludwig, M., Xu, W., Adamson, E. D., Wang, N. and Ezzell, R. M. (1998). Differences in elasticity of vinculin-deficient F9 cells measured by magnetometry and atomic force microscopy. *Exp. Cell Res.* **239**, 235-242.
Goldmann, W. H., Auernheimer, V., Thievessen, I. and Fabry, B. (2013). Vinculin, cell mechanics and tumour cell invasion. *Cell Biol. Int.* **37**, 397-405.
Golji, J., Lam, J. and Mofrad, M. R. K. (2011). Vinculin activation is necessary for complete talin binding. *Biophys. J.* **100**, 332-340.
Golji, J., Wendorff, T. and Mofrad, M. R. K. (2012). Phosphorylation primes vinculin for activation. *Biophys. J.* **102**, 2022-2030.
Grashoff, C., Hoffman, B. D., Brenner, M. D., Zhou, R., Parsons, M., Yang, M. T., McLean, M. A., Sligar, S. G., Chen, C. S., Ha, T. et al. (2010). Measuring mechanical tension across vinculin reveals regulation of focal adhesion dynamics. *Nature* **466**, 263-266.
Harburger, D. S. and Calderwood, D. A. (2009). Integrin signalling at a glance. *J. Cell Sci.* **122**, 159-163.
Hildebrandt, J. (1969). Comparison of mathematical models for cat lung and viscoelastic balloon derived by Laplace transform methods from pressure-volume data. *Bull. Math. Biophy.* **31**, 651-667.
Huang, Y., Zhang, W. and Gunst, S. J. (2011). Activation of vinculin induced by cholinergic stimulation regulates contraction of tracheal smooth muscle tissue. *J. Biol. Chem.* **286**, 3630-3644.
Huang, Y., Day, R. N. and Gunst, S. J. (2014). Vinculin phosphorylation at Tyr1065 regulates vinculin conformation and tension development in airway smooth muscle tissues. *J. Biol. Chem.* **289**, 3677-3688.
Humphries, J. D., Wang, P., Streuli, C., Geiger, B., Humphries, M. J. and Ballestrem, C. (2007). Vinculin controls focal adhesion formation by direct interactions with talin and actin. *J. Cell Biol.* **179**, 1043-1057.
Ito, S., Werth, D. K., Richert, N. D. and Pastan, I. (1983). Vinculin phosphorylation by the src kinase. Interaction of vinculin with phospholipid vesicles. *J. Biol. Chem.* **258**, 14626-14631.
Izard, T. and Vonrhein, C. (2004). Structural basis for amplifying vinculin activation by talin. *J. Biol. Chem.* **279**, 27667-27678.
Izard, T., Evans, G., Borgon, R. A., Rush, C. L., Bricogne, G. and Bois, P. R. J. (2004). Vinculin activation by talin through helical bundle conversion. *Nature* **427**, 171-175.
Janssen, M. E. W., Kim, E., Liu, H., Fujimoto, L. M., Bobkov, A., Volkmann, N. and Hanein, D. (2006). Three-dimensional structure of vinculin bound to actin filaments. *Mol. Cell* **21**, 271-281.
Jockusch, B. M. and Rüdiger, M. (1996). Crosstalk between cell adhesion molecules: vinculin as a paradigm for regulation by conformation. *Trends Cell Biol.* **6**, 311-315.
Johnson, R. P. and Craig, S. W. (1995). F-actin binding site masked by the intramolecular association of vinculin head and tail domains. *Nature* **373**, 261-264.
Kanchanawong, P., Shtengel, G., Pasapera, A. M., Ramko, E. B., Davidson, M. W., Hess, H. F. and Waterman, C. M. (2010). Nanoscale architecture of integrin-based cell adhesions. *Nature* **468**, 580-584.
Kasza, K. E., Nakamura, F., Hu, S., Kollmannsberger, P., Bonakdar, N., Fabry, B., Stossel, T. P., Wang, N. and Weitz, D. A. (2009). Filamin A is essential for active cell stiffening but not passive stiffening under external force. *Biophys. J.* **96**, 4326-4335.
Kollmannsberger, P. and Fabry, B. (2007). High-force magnetic tweezers with force feedback for biological applications. *Rev. Sci. Instrum.* **78**, 114301.
Kollmannsberger, P., Mierke, C. T. and Fabry, B. (2011). Nonlinear viscoelasticity of adherent cells is controlled by cytoskeletal tension. *Soft Matter* **7**, 3127-3132.
Küpper, K., Lang, N., Möhl, C., Kirchgessner, N., Born, S., Goldmann, W. H., Merkel, R. and Hoffmann, B. (2010). Tyrosine phosphorylation of vinculin at position 1065 modifies focal adhesion dynamics and cell tractions. *Biochem. Biophys. Res. Commun.* **399**, 560-564.
Marg, S., Winkler, U., Sestu, M., Himmel, M., Schönherr, M., Bär, J., Mann, A., Moser, M., Mierke, C. T., Rottner, K. et al. (2010). The vinculin-DeltaIn20/21 mouse: characteristics of a constitutive, actin-binding deficient splice variant of vinculin. *PLoS ONE* **5**, e11530.
Mierke, C. T., Kollmannsberger, P., Paranhos Zitterbart, D., Smith, J., Fabry, B. and Goldmann, W. H. (2008). Mechano-coupling and regulation of contractility by the vinculin tail domain. *Biophys. J.* **94**, 661-670.
Mierke, C. T., Kollmannsberger, P., Zitterbart, D. P., Diez, G., Koch, T. M., Marg, S., Ziegler, W. H., Goldmann, W. H. and Fabry, B. (2010). Vinculin facilitates cell invasion into three-dimensional collagen matrices. *J. Biol. Chem.* **285**, 13121-13130.
Moese, S., Selbach, M., Brinkmann, V., Karlas, A., Haimovich, B., Backert, S. and Meyer, T. F. (2007). The Helicobacter pylori CagA protein disrupts matrix adhesion of gastric epithelial cells by dephosphorylation of vinculin. *Cell. Microbiol.* **9**, 1148-1161.
Pelham, R. J., Jr and Wang, Y.-l. (1997). Cell locomotion and focal adhesions are regulated by substrate flexibility. *Proc. Natl. Acad. Sci. USA* **94**, 13661-13665.
Peng, X., Maiers, J. L., Choudhury, D., Craig, S. W. and DeMali, K. A. (2012). alpha-Catenin uses a novel mechanism to activate vinculin. *J. Biol. Chem.* **287**, 7728-7737.
Riveline, D., Zamir, E., Balaban, N. Q., Schwarz, U. S., Ishizaki, T., Narumiya, S., Kam, Z., Geiger, B. and Bershadsky, A. D. (2001). Focal contacts as mechanosensors: externally applied local mechanical force induces growth of focal contacts by an mDia1-dependent and ROCK-independent mechanism. *J. Cell Biol.* **153**, 1175-1186.
Subauste, M. C., Pertz, O., Adamson, E. D., Turner, C. E., Junger, S. and Hahn, K. M. (2004). Vinculin modulation of paxillin-FAK interactions regulates ERK to control survival and motility. *J. Cell Biol.* **165**, 371-381.
Thievessen, I., Thompson, P. M., Berlemont, S., Plevock, K. M., Plotnikov, S. V., Zemljic-Harpf, A., Ross, R. S., Davidson, M. W., Danuser, G., Campbell, S. L. et al. (2013). Vinculin-actin interaction couples actin retrograde flow to focal adhesions, but is dispensable for focal adhesion growth. *J. Cell Biol.* **202**, 163-177.
Tolbert, C. E., Thompson, P. M., Superfine, R., Burridge, K. and Campbell, S. L. (2014). Phosphorylation at Y1065 in vinculin mediates actin bundling, cell spreading, and mechanical responses to force. *Biochemistry* **53**, 5526-5536.
Wang, N., Tolic-Norrelykke, I. M., Chen, J., Mijailovich, S. M., Butler, J. P., Fredberg, J. J. and Stamenovic, D. (2002). Cell prestress. I. Stiffness and prestress are closely associated in adherent contractile cells. *Am. J. Physiol. Cell Phsiol.* **282**, C606-C616.
Winkler, J., Lünsdorf, H. and Jockusch, B. M. (1996). The ultrastructure of chicken gizzard vinculin as visualized by high-resolution electron microscopy. *J. Struct. Biol.* **116**, 270-277.
Zhang, Z., Izaguirre, G., Lin, S.-Y., Lee, H. Y., Schaefer, E. and Haimovich, B. (2004). The phosphorylation of vinculin on tyrosine residues 100 and 1065, mediated by SRC kinases, affects cell spreading. *Mol. Biol. Cell* **15**, 4234-4247.
Ziegler, W. H., Liddington, R. C. and Critchley, D. R. (2006). The structure and regulation of vinculin. *Trends Cell Biol.* **16**, 453-460.